Dalton Transactions

ROYAL SOCIETY OF CHEMISTRY

PAPER

View Article Online
View Journal | View Issue

Cite this: *Dalton Trans.*, 2026, **55**, 4097

A low-spin manganese(II) complex with an emissive charge-transfer excited state

Maxwell C. Rhames, †‡[a] Nora L. Burnett,‡[b] Annemarie A. Lee,[b] Colin B. Clark,[b] William C. Tocco, [a] Ahshabibi Ahmed,[b] Alexander N. Ruhren,[b] Claire Besson, [b] Julien A. Panetier, [b] John R. Swierk *[b] and Daniela M. Arias-Rotondo *[a]

Received 15th December 2025,
Accepted 7th February 2026

DOI: 10.1039/d5dt02990b

rsc.li/dalton

Manganese is an attractive earth-abundant metal for chromophores because it has multiple oxidation states, making it well-suited for photochemical applications involving electron transfer reactivity. Unfortunately, the tendency of manganese(II) to form high-spin complexes with metal-centered excited states has limited its viability. Herein, we disclose an air-stable $S = 1/2$ Mn(II) complex with N-heterocyclic carbene ligands. Spectroscopy revealed panchromatic absorption with two main bands in the visible region (with maxima at 480 nm and 580 nm), which have mixed charge-transfer and metal-centered character. Excitation into the low-energy band leads to an emissive state with a maximum at 770 nm (QY = 5.7×10^{-4}). Time-resolved emission spectroscopy revealed biphasic kinetics for the ground state recovery and a lifetime of 480 ps.

Introduction

Transition metal coordination compounds with charge-separated excited states that are accessible with visible light have been studied for decades in the context of photovoltaics, solar energy conversion, and photoredox catalysis, among other applications.[1] Traditionally, complexes of Ru(II), Ir(III), Re(I), and Os(II) have been the main focus of this research, due to their stability in solution, synthetic tunability, and long-lived metal-to-ligand charge transfer (MLCT) excited states.[1–3] The cost of these metals, however, has prompted researchers to explore earth-abundant alternatives.[4–6] As a result, first-row transition metals have received much attention, but while their MLCT states can be accessed with visible light, they tend to be deactivated through short-lived, low-energy ligand-field (LF) states.[6,7] In this context, N-heterocyclic carbenes (NHCs)[8] are an attractive class of ligands: they are strongly sigma-donating, which helps destabilize the LF states and thus extend the MLCT lifetimes.[9] Using NHC ligands, the groups of Sundström, Wärnmark, Haacke, and Gros have disclosed some Fe(II) complexes with record-breaking MLCT lifetimes[9–11] and Wenger and co-workers have reported a Co(III) complex with NHCs whose lowest-energy excited state is an MLCT with a 1.2 ns lifetime.[12]

Manganese has emerged as an attractive earth-abundant metal for chromophores: its numerous available oxidation states make it well-suited for applications involving electron transfer reactivity. Of the seven oxidation states available to manganese, the +1 and +4 have shown promise: Mn(I) complexes can access MLCT excited states like other d^6 metals, as Wenger and his group reported;[13] Heinze and her group recently disclosed a Mn(I) complex with a record MLCT lifetime using NHC ligands.[14] On the other hand, Mn(IV) complexes can access LMCT states, as initially demonstrated by the Reber, Jackson, Smith and Telser groups.[15] Work by the Heinze group[16] as well as by the Smith, Jakubikova, and Hammarström groups,[17] has shown that these LMCT states can be powerful photooxidants. A drawback of many Mn(I) complexes is that they are air-sensitive; conversely, Mn(IV) complexes may be air-stable, but their syntheses usually require strong oxidants. Interestingly, manganese is most stable in its +2 oxidation state, but its tendency to form high-spin complexes[18] without low-lying MLCT states[19] has drastically limited the viability of Mn(II)-based chromophores. The vast majority of the Mn(II) literature focuses on solid-state materials featuring high-spin Mn(II) and whose luminescence is due to the $^4T_1$ to $^6A_1$ metal-centered transition.[20–24] Preparing benchstable, low-spin Mn(II) complexes that absorb visible light in solution to access a charge-separated excited state remains a challenge. We hypothesized that this could be achieved using NHC ligands, as their sigma-donating character would increase the energy of the LF (metal-centered) states, forcing

[a]*Department of Chemistry and Biochemistry, Kalamazoo College, Kalamazoo, MI 49006, USA. E-mail: dariasr@kzoo.edu*
[b]*Department of Chemistry, Binghamton University (SUNY), Binghamton, NY 13902, USA. E-mail: jswierk@binghamton.edu*
†Current address: Department of Chemistry and Biochemistry, University of Delaware; Newark, DE 19716, United States of America.
‡These authors contributed equally to this work.

the Mn(II) center into a low-spin configuration. In particular, NHC ligands with an extended conjugated system could help stabilize the excited electron of an MLCT state.

Herein, we report $[Mn(bim^{Ph})_2](PF_6)_2$ (bim^{Ph} is 2,6-bis[3-phenylimidazol-2-ylidene]pyridine), an air-stable Mn(II) complex with the rare $S = \frac{1}{2}$ (low-spin) electronic configuration[25–28] and, to the best of our knowledge, the first Mn(II) compound with only NHC ligands in its coordination sphere.[29–31] $[Mn(bim^{Ph})_2](PF_6)_2$ absorbs visible light over a broad wavelength range to access two charge-transfer excited states, which seem to behave independently of each other. While the excited-state lifetime of $[Mn(bim^{Ph})_2](PF_6)_2$ is shorter than what is necessary for bimolecular reactivity in solution, this work opens the door to using manganese(II) complexes as chromophores for light-driven applications.

Results and discussion

Synthesis, structure, and ground state characterization

The title compound was obtained through the deprotonation of the bis-imidazolium ligand precursor $[H_2bim^{Ph}](PF_6)_2$ [32] and its subsequent reaction with $Mn(OTf)_2$, adapting procedures developed for iron(II) analogues.[10] Our procedure is consistent with what was reported by Heinze and colleagues.[14] The X-ray structure of $[Mn(bim^{Ph})_2](PF_6)_2$ (CCDC 2420773) revealed that both ligands exist perpendicular to each other in a meridional fashion with the metal center exhibiting a distorted octahedral geometry (Fig. 1). To date, only one structurally comparable Mn(II) complex has been reported: $Mn(bim^{Dipp})Br_2$, where bim^{Dipp} is 2,6-bis[3-(2,6-diisopropylphenyl)imidazol-2-ylidene]pyridine.[33] Comparing the crystal structures of both complexes reveals some striking differences: the Mn–C bonds in $[Mn(bim^{Ph})_2]^{2+}$ range from 1.982(5) to 1.997(5) Å and their Mn–N counterparts are 1.957(4) and 1.958(4) Å, respectively. In contrast, $Mn(bim^{Dipp})Br_2$ has Mn–C bond lengths of 2.206(2) and 2.210(2) Å and 2.2574(16) Å for Mn–N. While the bulkier Dipp capping groups may contribute to longer Mn–ligand bonds, a difference of more than 0.2 Å is unlikely to derive solely from the difference in capping ligands. These values are in line with the reported changes in the high-spin-to-low-spin difference in metal ion radii.[34] The shorter bond lengths in $[Mn(bim^{Ph})_2]^{2+}$ are consistent with this complex having a low-spin Mn(II) center; this is supported by magnetic data, as discussed below.

Solution-phase magnetic susceptibility measurements in acetonitrile using the Evans method[35] revealed that the effective magnetic moment (μ_{eff}) of $[Mn(bim^{Ph})_2](PF_6)_2$ is $1.9\mu_B$ (Fig. S1). This value agrees with previously reported low-spin Mn(II) examples, which are in the 1.65–2.17μ_B range,[25–28] indicating that the Mn(II) center exists in a $S = \frac{1}{2}$ spin state. This low-spin d^5 configuration is rare for first-row transition metals; in the case of Mn(II), many of these compounds quickly decompose in solution.[36,37] In contrast, $[Mn(bim^{Ph})_2](PF_6)_2$ is air-stable in acetonitrile solution for several days, and indefinitely air-stable in the solid state.

The electronic absorption spectrum of $[Mn(bim^{Ph})_2](PF_6)_2$ shows ligand-centered (LC) bands at wavelengths shorter than 400 nm, which are also observed for the ligand in solution (Fig. 2). The spectrum also exhibits two broad absorption bands in the visible region that peak at approximately 480 and 580 nm, with molar absorption coefficients of 4400 and 5600 M^{-1} cm^{-1}, respectively. These values are consistent with those of charge-transfer transitions.[38,39] This assignment is further supported by electrochemistry and computational results (*vide infra*).

Cyclic voltammetry in acetonitrile revealed two sets of quasi-reversible waves attributable to the metal center (Fig. S7). The first, at −0.15 V *vs.* Fc/Fc^+, can be assigned to the $Mn^{III/II}$ redox couple[40] whereas the second, at −1.01 V *vs.* Fc/Fc^+, can be attributed to the $Mn^{II/I}$ reduction; these values agree with those reported by Heinze and co-workers for a struc-

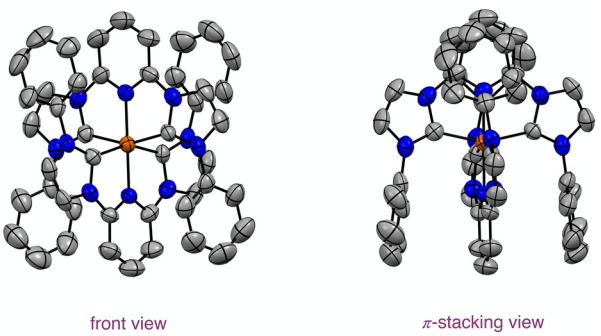

Fig. 1 ORTEP drawing of $[Mn(bim^{Ph})_2](PF_6)_2$ obtained from a single-crystal X-ray structure determination. Thermal ellipsoids are shown at 50% probability. Hydrogen atoms and PF_6^- ions are omitted for clarity. Color code: C (gray), N (blue), Mn (orange). Left image illustrates the front view of the structure; the right image highlights the π-stacking between the phenyl and pyridine rings.

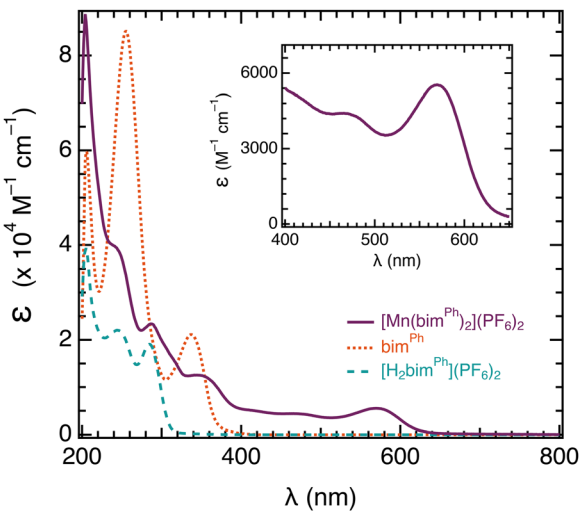

Fig. 2 Electronic absorption spectra of $[Mn(bim^{Ph})_2](PF_6)_2$ (solid purple), $[H_2bim^{Ph}](PF_6)_2$ (dashed green), and bimPh (dotted orange). All spectra were collected in acetonitrile.

turally related Mn(I) complex.[14] We have not observed peaks that could be assigned to ligand processes. However, for ligands structurally related to bim^{Ph}, oxidation waves ranging from 1.1 to 1.2 V (*vs.* Fc/Fc$^+$) have been reported;[41] conversely, reduction events near −2 V (*vs.* Fc/Fc$^+$) have also been observed.[11] These experimental data can be used to estimate the energy of a charge-transfer transition. Comparing the redox potentials of the reversible Mn$^{III/II}$ couple with that of the irreversible ligand reduction to simulate a MLCT suggests that this process would require approximately 2 eV, or roughly 620 nm light. A similar process can be used to evaluate the energetics of a LMCT by using the redox potentials of the Mn$^{II/I}$ couple and irreversible ligand oxidation. This estimation suggests that this transition would require 2.1 eV, or 590 nm light. Hence, these redox potentials are consistent with low-energy charge-transfer excited states. A recent report of a structurally related Mn(II) complex assigns these transitions as MLCT,[42] which agrees with our computational results, as discussed below.

Emission spectroscopy: steady-state and time-resolved experiments

The steady-state emission spectrum for [Mn(bim^{Ph})$_2$](PF$_6$)$_2$ in acetonitrile solution is shown in Fig. 3. Excitation into the band at 600 nm gives rise to a broad emission band that peaks around 770 nm (QY = 5.7 × 10^{-4}; see SI). The excitation spectrum for this emission band shows that this excited state is only accessible through excitation at redder wavelengths (530 through 610 nm; see Fig. 3). A second emission band is observed at 620 nm upon excitation into the higher absorption band of [Mn(bim^{Ph})$_2$](PF$_6$)$_2$ (λ_{exc} 450–480 nm).

A representative time-resolved emission trace for [Mn(bim^{Ph})$_2$](PF$_6$)$_2$ in acetonitrile is shown in Fig. 4. Excitation at 585 nm (λ_{em} = 750–770 nm) results in a biexponential decay, with τ_1 < 60 ps (close to the IRF) and τ_2 = 480 ps. This longer-lived component may be able to engage in bimolecular reactivity in solution, as demonstrated for Fe(II) complexes with similar ligands.[43] Furthermore, understanding the nature of this excited state can lead to strategies to extend its lifetime *via* synthetic modifications.

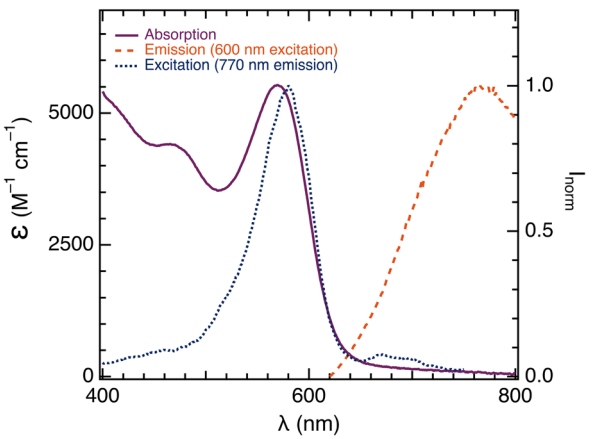

Fig. 3 Steady-state emission spectrum of [Mn(bim^{Ph})$_2$](PF$_6$) for λ_{exc} = 600 nm (dashed orange trace). The dotted blue trace is the excitation spectrum for λ_{em} = 770 nm. The solid purple trace is the electronic absorption spectrum. All spectra were collected in acetonitrile solution under air.

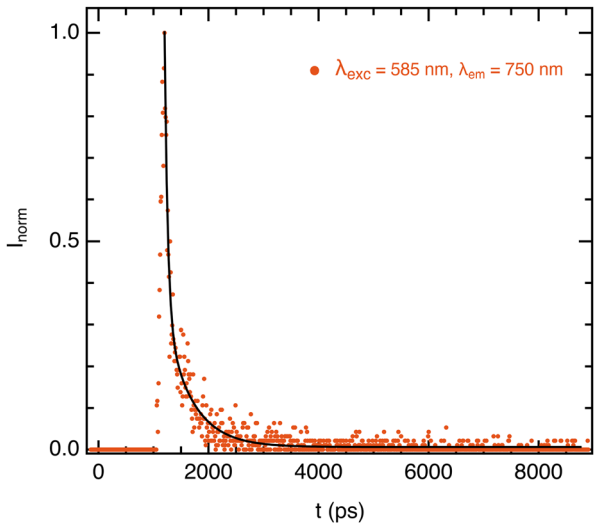

Fig. 4 Time-resolved emission spectrum of [Mn(bim^{Ph})$_2$](PF$_6$)$_2$ collected in acetonitrile. This representative decay trace is for λ_{exc} = 585 nm and λ_{em} = 750 nm (τ_1 < 60 ps and τ_2 = 480 ± 20 ps). The data are fitted with a double exponential (black line). See SI for details.

Though our data suggest that [Mn(bim^{Ph})$_2$](PF$_6$)$_2$ can access two separate excited states upon visible light absorption, it is uncommon for transition metal complexes to access two independent excited states. We are carrying out additional experiments to determine if this emission is due to an impurity or if it can be attributed to our Mn(II) compound; discussion of our results so far can be found in the SI. In addition, our computational results provide some insight into the nature of such excited states (see below).

Computational results

We performed density functional theory (DFT) calculations to probe the ground-state electronic structure of [Mn(bim^{Ph})$_2$]$^{2+}$. Based on the computed electronic energies, our computational results suggest that the doublet and sextet states are within 3.8 kcal mol^{-1} of each other (Table S6). However, the calculated bond distances for the low-spin doublet are in better agreement. For example, the computed Mn–C and Mn–N bonds are within 0.04 Å of the experimental values (Table S7). This suggests that [Mn(bim^{Ph})$_2$]$^{2+}$ is best described as a doublet ground state, in agreement with our solution-phase magnetic susceptibility measurements. In contrast, the computed Mn–N bond distance for the sextet state is significantly elongated (*e.g.*, Mn–N = 2.48 Å, Table S9), which allows for the stabilization of the d_{z^2} orbital.

We also performed time-dependent DFT (TD-DFT) to probe the electronic configurations of the excited states and to provide a hypothesis for the two experimentally accessible excited states. We focus on the computed excited states in the

400–600 nm region and compare them to the electronic absorption spectrum of the complex (Fig. S13). As shown by plotting the natural transition orbitals (NTOs), we observe numerous MLCT transitions between 400 and 600 nm (Fig. S14 and S15). Surprisingly, our TD-DFT calculations reveal a significant similarity among the MLCT excitations, with all transitions exhibiting $(t_{2g}) \rightarrow \pi^*(py)$ character (Fig. S14 and S15). This suggests that the difference between the two absorption bands cannot be explained solely by their MLCT character.

Instead, we hypothesize that the different absorption bands arise from excited states that have mixed MLCT and metal-centered character (Fig. 5). At λ_{calc} = 597 nm, the TD-DFT calculations implicate $d_{xz}(t_{2g}) \rightarrow d_{z^2}(e_g)$. The $d_{z^2}(e_g)$ exhibits antibonding character and is ideally positioned to interact with the pyridine ligands. Thus, we propose that the excited state at approximately 580 nm involves a significant elongation of the Mn–N(py) bond, leading to a lower-energy species. This observation is also consistent with the sextet state being competitive with the doublet ground state upon dissociation of the Mn–N bonds, stabilizing the d_{z^2} orbital. In contrast, visualization of the key NTOs at λ_{calc} = 416 nm shows that excitation is into the $d_{x^2-y^2}$ orbital. This orbital is positioned to interact with the imidazole rings but not the pyridines (Fig. 5). Because of the strong σ-donor character of NHC moieties, they are less prone to dissociation, suggesting that the excited state arising from 480 nm excitation is not subjected to the same Mn–N(py) bond elongation and remains at a higher energy.

Our results agree with those reported by the Heinze group:[14] both Mn(I) and Mn(II) complexes with these NHC ligands display two MLCT absorption bands that involve only the pyridine ring, not the imidazole. This is consistent with the anionic carbon making the imidazole ring harder to reduce. In contrast, Fe(II) complexes with NHC ligands[9–11] also display two MLCT bands, but the higher energy one has been assigned as ML(imidazole)CT, while the lower energy excited state is an ML(pyridine)CT.

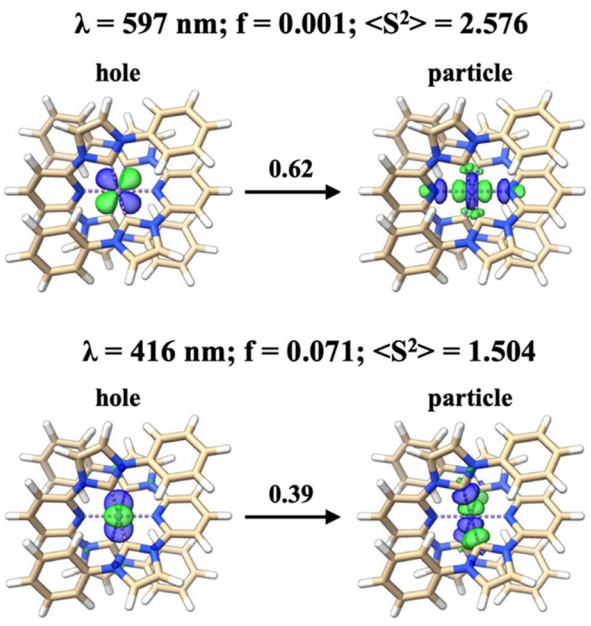

Fig. 5 Isosurface plots of the metal-centered transitions at λ_{calc} = 597 nm (top) and 416 nm (bottom).

Conclusions

We have reported a rare example of a low-spin, air stable Mn(II) complex with NHC ligands. This compound absorbs visible light over a wide range of wavelengths, with maxima at 480 nm and 580 nm: we have assigned both of these bands as MLCT transitions through a combination of electrochemical and computational studies. Remarkably, only excitation into the lower-energy band leads to emission with a maximum at 770 nm. This excited state decays with biexponential kinetics, with the longer-lived component having a lifetime of 480 ps. A second emission, which at present appears to be authentic to the complex, is also observed at 620 nm upon excitation into the higher energy absorption bands. Based on computational analysis, we hypothesize that the key difference between these two excited states arises from distinct metal-centered excitations involving different d orbitals in the e_g manifold. The lower energy band is predicted to involve excitation to the $d_{z^2}(e_g)$ state, which would elongate the Mn–N bonds, lowering the excited-state energy and allowing access to the shorter-lived S = 5/2 manifold. In contrast, the higher energy band is predicted to involve $d_{x^2-y^2}(e_g)$, which does not result in Mn–N bond elongation and remains higher in energy in the S = 1/2 state. Work is underway to further probe the mechanisms of ground-state recovery for each excited state.

Author contributions

D. M. A. R. and J. R. S. designed the project. M. C. R. and W. C. T. synthesized the compounds. M. C. R., A. A. L., C. B. C., A. A., A. N. R. and C. B. collected and analyzed experimental data. N. L. B. and J. A. P. carried out the computational work. All authors interpreted the results and contributed to writing the manuscript.

Conflicts of interest

There are no conflicts to declare.

Data availability

The data that support the findings of this study are openly available in figshare at https://doi.org/10.6084/m9.figshare.31267495.

Supplementary information (SI): synthetic procedures, materials and methods, computational details and results, and additional characterization data (PDF). See DOI: https://doi.org/10.1039/d5dt02990b.

CCDC 2420773 for $[Mn(bim^{Ph})_2](PF_6)_2$ contains the supplementary crystallographic data for this paper.[44]

Acknowledgements

We thank Jasmine A. Ivy for preliminary work on the synthesis of the ligand. We are deeply grateful to Dr Gary J. Blanchard for his assistance with TCSPC measurements. This material is based upon work supported by the National Science Foundation under Grants: CHE-2316810 (DMAR), CHE-2400072 (JAP), and CHE-2047492 (JRS).

References

1 D. M. Arias-Rotondo and J. K. McCusker, *Chem. Soc. Rev.*, 2016, **45**, 5803–5820.
2 A. Juris, V. Balzani, F. Barigelletti, S. Campagna, P. Belser and A. von Zelewsky, *Coord. Chem. Rev.*, 1988, **84**, 85–277.
3 I. M. Dixon, J.-P. Collin, J.-P. Sauvage, L. Flamigni, S. Encinas and F. Barigelletti, *Chem. Soc. Rev.*, 2000, **29**, 385–391.
4 O. S. Wenger, *J. Am. Chem. Soc.*, 2018, **140**, 13522–13533.
5 C. B. Larsen and O. S. Wenger, *Chem. – Eur. J.*, 2018, **24**, 2039–2058.
6 C. Förster and K. Heinze, *Chem. Soc. Rev.*, 2020, **49**, 1057–1070.
7 J. K. McCusker, *Science*, 2019, **363**, 484–488.
8 H. V. Huynh, *Chem. Rev.*, 2018, **118**, 9457–9492.
9 Y. Liu, T. Harlang, S. E. Canton, P. Chábera, K. Suárez-Alcántara, A. Fleckhaus, D. A. Vithanage, E. Göransson, A. Corani, R. Lomoth, V. Sundström and K. Wärnmark, *Chem. Commun.*, 2013, **49**, 6412.
10 T. Duchanois, T. Etienne, C. Cebrián, L. Liu, A. Monari, M. Beley, X. Assfeld, S. Haacke and P. C. Gros, *Eur. J. Inorg. Chem.*, 2015, **2015**, 2469–2477.
11 L. Liu, T. Duchanois, T. Etienne, A. Monari, M. Beley, X. Assfeld, S. Haacke and P. C. Gros, *Phys. Chem. Chem. Phys.*, 2016, **18**, 12550–12556.
12 N. Sinha, B. Pfund, C. Wegeberg, A. Prescimone and O. S. Wenger, *J. Am. Chem. Soc.*, 2022, **144**, 9859–9873.
13 P. Herr, C. Kerzig, C. B. Larsen, D. Häussinger and O. S. Wenger, *Nat. Chem.*, 2021, **13**, 956–962.
14 S. Kronenberger, R. Naumann, C. Förster, N. R. East, J. Klett and K. Heinze, *Nat. Commun.*, 2025, **16**, 7850.
15 V. Baslon, J. P. Harris, C. Reber, H. E. Colmer, T. A. Jackson, A. P. Forshaw, J. M. Smith, R. A. Kinney and J. Telser, *Can. J. Chem.*, 2017, **95**, 547–552.
16 N. R. East, R. Naumann, C. Förster, C. Ramanan, G. Diezemann and K. Heinze, *Nat. Chem.*, 2024, **16**, 827–834.
17 N. Kaul, E. Asempa, J. A. Valdez-Moreira, J. M. Smith, E. Jakubikova and L. Hammarström, *J. Am. Chem. Soc.*, 2024, **146**, 24619–24629.
18 M.-N. Collomb and A. Deronzier, in *Encyclopedia of Inorganic and Bioinorganic Chemistry*, ed. R. A. Scott, John Wiley & Sons, Ltd., 2011.
19 M. Wang, J. England, T. Weyhermüller and K. Wieghardt, *Inorg. Chem.*, 2014, **53**, 2276–2287.
20 M. Bortoluzzi, J. Castro, F. Enrichi, A. Vomiero, M. Busato and W. Huang, *Inorg. Chem. Commun.*, 2018, **92**, 145–150.
21 M. Bortoluzzi, J. Castro, A. Gobbo, V. Ferraro, L. Pietrobon and S. Antoniutti, *New J. Chem.*, 2020, **44**, 571–579.
22 M. Bortoluzzi, V. Ferraro and J. Castro, *Dalton Trans.*, 2021, **50**, 3132–3136.
23 A. V. Artem'ev, M. P. Davydova, M. I. Rakhmanova, I. Yu. Bagryanskaya and D. P. Pishchur, *Inorg. Chem. Front.*, 2021, **8**, 3767–3774.
24 A. S. Berezin, D. G. Samsonenko, V. K. Brel and A. V. Artem'Ev, *Dalton Trans.*, 2018, **47**, 7306–7315.
25 S. Karmakar, S. B. Choudhury and A. Chakravorty, *Inorg. Chem.*, 1994, **33**, 6148–6153.
26 S. Ganguly, S. Karmakar, C. K. Pal and A. Chakravorty, *Inorg. Chem.*, 1999, **38**, 5984–5987.
27 A. Saha, P. Majumdar and S. Goswami, *J. Chem. Soc., Dalton Trans.*, 2000, 1703–1708.
28 M. D. Walter, C. D. Sofield, C. H. Booth and R. A. Andersen, *Organometallics*, 2009, **28**, 2005–2019.
29 R. A. Layfield, *Chem. Soc. Rev.*, 2008, **37**, 1098.
30 S. J. Hock, L.-A. Schaper, W. A. Herrmann and F. E. Kühn, *Chem. Soc. Rev.*, 2013, **42**, 5073.
31 V. Charra, P. de Frémont and P. Braunstein, *Coord. Chem. Rev.*, 2017, **341**, 53–176.
32 E. Peris, J. Mata, J. A. Loch and R. H. Crabtree, *Chem. Commun.*, 2001, 201–202.
33 D. Pugh, J. A. Wright, S. Freeman and A. A. Danopoulos, *Dalton Trans.*, 2006, 775–782.
34 R. D. Shannon, *Acta Crystallogr., Sect. A*, 1976, **32**, 751–767.
35 D. F. Evans, *J. Chem. Soc.*, 1959, 2003–2005.
36 P. H. Rieger, *Coord. Chem. Rev.*, 1994, **135–136**, 203–286.
37 K. R. Mann, M. Cimolino, G. L. Geoffroy, G. S. Hammond, A. A. Orio, G. Albertin and H. B. Gray, *Inorg. Chim. Acta*, 1976, **16**, 97–101.
38 A. B. P. Lever, *J. Chem. Educ.*, 1974, **51**, 612.
39 R. S. Drago, *Physical Methods for Chemists*, Saunders College Pub., Philadelphia, 1992.
40 N. R. East, C. Förster, L. M. Carrella, E. Rentschler and K. Heinze, *Inorg. Chem.*, 2022, **61**, 14616–14625.
41 Y. Vukadinovic, L. Burkhardt, A. Päpcke, A. Miletic, L. Fritsch, B. Altenburger, R. Schoch, A. Neuba, S. Lochbrunner and M. Bauer, *Inorg. Chem.*, 2020, **59**, 8762–8774.
42 S. Kronenberger, R. Naumann, C. Förster, J. Klett, D. Schollmeyer, L. M. Carrella, E. Rentschler and K. Heinze, *ChemRxiv*, 2025, DOI: 10.26434/chemrxiv-2025-lrnqm, preprint.
43 J. Wellauer, F. Ziereisen, N. Sinha, A. Prescimone, A. Velić, F. Meyer and O. S. Wenger, *J. Am. Chem. Soc.*, 2024, **146**, 11299–11318.
44 CCDC 2420773: Experimental Crystal Structure Determination, 2025, DOI: 10.5517/ccdc.csd.cc2m80gd.